



HAL
open science

J-integral based fracture toughness of 15Cr-5Ni stainless steel during phase transformation

Liu Jingde, Michel Coret, Alain Combescure, Philippe Chaudet

► To cite this version:

Liu Jingde, Michel Coret, Alain Combescure, Philippe Chaudet. J-integral based fracture toughness of 15Cr-5Ni stainless steel during phase transformation. *Engineering Fracture Mechanics*, 2012, 96, pp.328-339. 10.1016/j.engfracmech.2012.08.001 . hal-01007003

HAL Id: hal-01007003

<https://hal.science/hal-01007003>

Submitted on 3 Jun 2017

HAL is a multi-disciplinary open access archive for the deposit and dissemination of scientific research documents, whether they are published or not. The documents may come from teaching and research institutions in France or abroad, or from public or private research centers.

L'archive ouverte pluridisciplinaire **HAL**, est destinée au dépôt et à la diffusion de documents scientifiques de niveau recherche, publiés ou non, émanant des établissements d'enseignement et de recherche français ou étrangers, des laboratoires publics ou privés.



Distributed under a Creative Commons Attribution 4.0 International License

J-integral based fracture toughness of 15Cr–5Ni stainless steel during phase transformation

Liu Jikai, M. Coret, A. Combescure, P. Chaudet

Université de Lyon, CNRS INSA-Lyon, LaMCoS UMR5259, F-69621 Villeurbanne, France

This paper proposes a simple effective method to extract the elastoplastic toughness J_{1C} from a simple experiment on a plate. The method is based on a combination of global experimental load displacement measurements, finite element simulation, and digital image correlation which is used to observe the crack propagation initiation as well as to determine the appropriate boundary conditions to be used in numerical simulation. This method is applied to obtain the J_{1C} value of material 15Cr–5Ni stainless steel, which is normally written as 15–5PH after different temperature histories. This paper investigates the influence of the different material state history on the mechanical properties due to the heat treatment and possible phase transformation. Meanwhile, the fractography is also analysed. The result of J_{1C} value shows that the pure martensite 15–5PH has higher fracture toughness at room temperature than at 200 °C. The toughness is also higher than the original material after one cycle heat treatment, which is probably caused by some residual austenite. Meanwhile, pure austenite 15–5PH has a higher fracture toughness than pure martensite 15–5PH at 200 °C. The J_{1C} value of the dual phase 15–5PH during the martensitic transformation also shows that possibly austenite can enhance the ductility of the material as well as fracture toughness.

Keywords:

Fracture toughness
Phase transformation
Critical *J*-integral
Boundary condition
Digital image correlation

1. Introduction

The research presented in this paper is linked to the basic problem of life extension for expensive components. The following problem is often encountered by the industry: a defect (or crack) is detected during the life of a component, what is the decision to take for metallic components: change the component or repair the crack? This is a recurrent question for aerospace parts and nuclear components as well as for railways carriages.

Crack reparation is attractive because it is less expensive, but it is very often not chosen for important components because people fear the consequences of this reparation on the future safety of the repaired component. The main reason is the important uncertainties on the final quality of the reparation such as new defect introduction, metallurgical changes and high residual stresses. If the crack root is still present after reparation, what happens to this initial damage during the repair (filling with welding material)? This research is devoted to the acquisition of basic understanding of what happens in such cases. The research presented in this paper is only focussed on getting basic information on the fracture material properties (toughness) in case of typical repair and refilling temperature histories. The following experimental tests are performed. A fatigue crack side is initiated in a thin plate. This plate is submitted to a typical uniform thermal history and the monotonic load crack propagation tests are performed on the plate. The objective of these tests is to evaluate quantitatively if the

Nomenclature

a	fatigue crack length
a_0	notch length of the fracture specimen
Ac_1	austenitic transformation start temperature
Ac_3	austenitic transformation finish temperature
α	martensite phase
α_α	dilatation coefficient of martensite phase
α_γ	dilatation coefficient of austenite phase
B	thickness of the fracture specimen
da	crack length difference between two fracture specimens
ΔW	different work between two fracture tests
$\Delta G_{\alpha \rightarrow \gamma}^{T_{ref}}$	different of compactness of phase α compared to phase γ at T_{ref}
E^{thm}	thermo metallurgical microscopic strain
F	force
G_θ	energy release rate method
γ	austenite phase
J_{1C}	critical J -integral in model I
M_f	martensite transformation finish temperature
M_s	martensite transformation start temperature
t	time
T	temperature
T_{ref}	reference temperature
$U_{(a)}$	potential after the fatigue test
$U_{(a_0)}$	potential before the fatigue test
$Z_\gamma(T)$	volume proportion of austenite phase

toughness is affected by the metallurgical state of the material, resulting from various temperature histories, and how much. Nevertheless the fracture specimen geometry is a thin plate which permits to get the same material characteristic on the crack front when the specimen is subjected to fast thermal transients. This results into non standard fracture toughness evaluation, the triaxiality of thin plate being rather low. The material chosen 15Cr–5Ni stainless steel (15–5PH) is a dual phase material which experiences phase transformation. Dilatometry tests permits to characterise this transformation. The evolution of standard material properties as yield stress or Young's modulus is evaluated using standard round bar monotonic testing submitted to the same thermal history.

1.1. Stainless steel: 15–5PH

The material 15–5PH (Condition H1025) is considered herein. 15–5PH is a martensitic precipitation hardening stainless steel which is a precipitation of age hardened and heat solution-treated material at 1025 °F for 4 h and then air cooling. It is widely used in aerospace and nuclear areas because its toughness and hardness are high and it has a good corrosion resistance when small quantity of alloying element is added [1]. Table 1 shows the chemical composition of 15–5PH.

1.2. Phase transformation in 15–5PH

Like others metals, 15–5PH experiences phase transformation during specific heat treatment. This material is in the family of dual phase ones because it only experiences austenite and martensitic transformation but no ferrite or pearlite transformation. The research on phase transformation effects on toughness is then easier. Fig. 1 displays the elongation curve of 15–5PH with a whole heat treatment cycle.

The test is done with an initial heating rate of +5 °C/s until the maximum temperature which is 900 °C. The first linear response is the expansion of martensite. At about 770 °C the austenite transformation starts and is finished at about 815 °C. After the maximum temperature 900 °C is reached the specimen is air-cooled. The first part of the decreasing curve is the linear contraction of austenite which stops at about 185 °C where martensitic transformation starts. The transformation is over at about 40 °C. Fig. 2 displays the measured temperatures loading during the test. The cooling rate is between 0.6 and 0.2 °C/s during the martensitic transformation.

Table 1

Chemical compositions of 15–5PH.

Element wt.%	Cr	Ni	Cu	C	Mn	Other alloys	Fe
	15.44	4.50	3.16	0.02	0.66	N/A	Balance

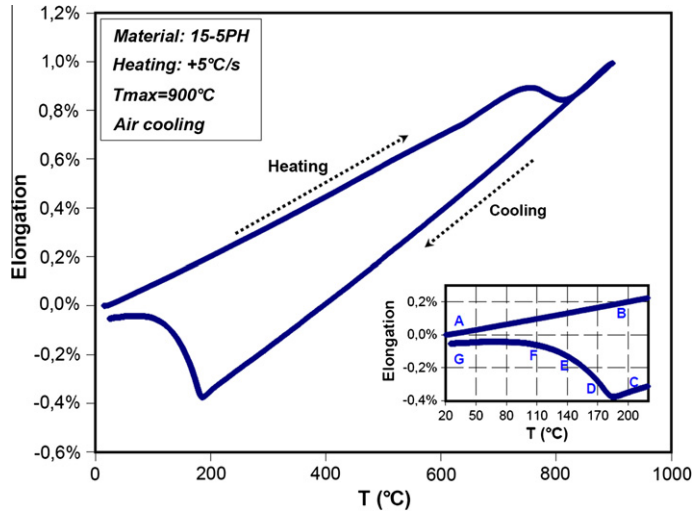


Fig. 1. Elongation during a heat loading cycle, heating rate: +5 °C/s, max temperature is 900 °C and air cooling.

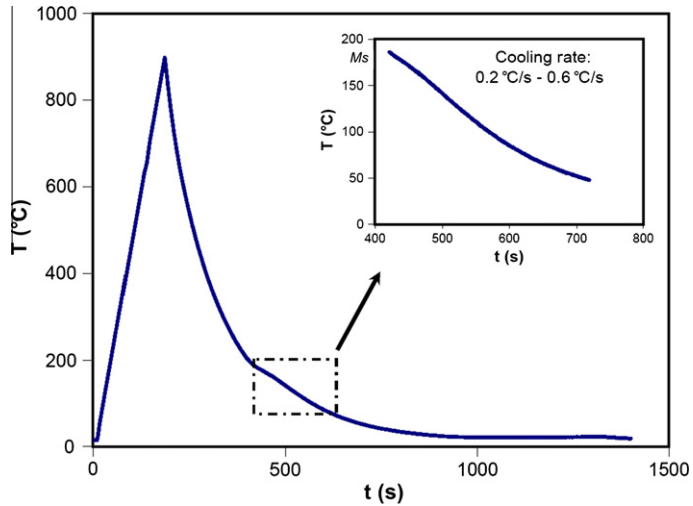


Fig. 2. Temperature history during a heat loading cycle and cooling rate during the martensitic transformation.

We will focus on the cooling martensitic transformation of 15-5PH to study the effect of metallurgical phase transformation on mechanical behaviour. One can read in [2] that the martensitic transformation of 15-5PH is temperature driven, that is to say, once the temperature stops decreasing the transformation will also stop. Our experimental results are consistent with this observation. This means that one can keep a constant phase proportion if the temperature is not changed during the martensitic transformation and do the corresponding mechanical test.

As indicated in the lower right corner of Fig. 1, we will study seven states of the material (points A–G). For example, points A and G are two tests performed at room temperature one before the heat treatment (A) and one after a whole cycle heat treatment (G). Point B is fully martensite at 200 °C while point C is totally austenite at the same temperature just before the martensitic transformation; Points D, E and F are three points during the martensitic transformation at 170, 140 and 110 °C. Table 2 shows the phase proportion at each point [1,3–5].

Table 2
Analysis points related to the phase.

Point	A	B	C	D	E	F	G
Phase	α	α	γ	α/γ	α/γ	α/γ	α
% of α	100%	100%	$\approx 0\%$	25%	60%	80%	$\approx 100\%$

Note: α presents martensite, γ presents austenite, α/γ means martensite and austenite mixed. The reason why there are two approximately equal symbols is that the phase transformation may be not completely finished, for example there may be some residual austenite exists at point G.

1.3. Effect of phase transformation on crack resistance

A lot of work has been done on the effect of phase transformation on material properties in the last half century. Greenwood, Johnson and Magee respectively worked on the effect of an applied stress during the phase transformation: they showed that this stress could lead to an additional irreversible strain [6,7], described by the phase TRansformation Induced Plasticity (TRIP). Furthermore, Bressanelli and Moskowitz presented that TRIP can increase the strain-hardening rate which results in an overall increase of tensile strength and uniform ductility [8]. Consequently the TRIP high strength steel came out [9]. Subsequently many papers appeared dealing with the influence of mechanically-induced martensitic transformation on the general mechanical behaviour of metastable austenitic steels under monotonic and cyclic loading [10]. For example, Gerberich et al. [11] and Antolovich and Singh [12] have researched the enhancement of fracture toughness due to TRIP phenomenon. Many constitutive equations and kinetic theories of isothermal martensitic transformation have been also presented [13,14]. Sun and Hwang established a micromechanics constitutive model based on an internal variable theory to describe the stress-strain-temperature relations during forward and reverse transformation processes [15]. Hannink et al., found that the stress-induced martensitic transformation in zirconia ceramics involves predominately positive volumetric change, resulting in a reduction in the crack-tip stress-intensity factor [16], which in turn leads to an increase in the material fracture toughness. By contrast, the phase transformation in shape memory alloys (SMAs) involves negative volumetric change, which would result in an increase in the crack-tip stress-intensity factor and thus a decrease in fracture toughness [17]. In this paper we will present the fracture toughness values before, during and after the martensitic transformation of 15-5PH. This will provide an input for the effect of phase transformation in 15-5PH on its crack propagation resistance.

1.4. Critical J -integral evaluation

Rice [18] showed that the energy rate interpretation of the J -integral is fundamental to elastic-plastic fracture toughness testing. Crack propagation initiates once the loading reaches a material-dependent critical J -integral value J_{1C} . In the last decades many experimental methods have been successfully proposed to get a robust value of J_{1C} ([19–24]). These experimental approaches impose to have specified specimen geometries and most of them are associated with rather expensive experiments. Moreover all these experimental methods can't be applied to the determination of J_{1C} in case of phase transformations situations, because one cannot ensure, with thick specimens that the temperature fields around the crack tip region within the specimen is uniform. This implies that one do not know what is the material state within the specimen and along the crack front without making complex 3D computations, which is heavy and debatable if not compared with ad hoc measures.

It was then decided to use a non conventional method to extract the J_{1C} value. The J_{1C} value is determined on the base of observation of crack propagation on thin cracked plane specimen. The method is first tested at room temperature for which the material is less ductile. The global load displacement curve was correlated with the Digital Image Correlation (DIC) [25,26] measures which give the crack tip position, the image processing of the two faces of the specimen which are used to check the previous prediction and the Johnson potential measures [27] which provide a third measure of the crack tip position. This comparison shows that the load decreases when the crack starts to propagate.

The J_{1C} value is extracted using a careful finite element analysis of the experiments. One could argue that this finite element computation can be avoided because DIC contains all the information. This is an interesting and efficient processing of the results but, in case of elastoplastic response, this method relies on the input of a stress strain law. It has been measured in our case and hence a purely experimental method could be directly applied. The interest of the chosen method is to cross check the use of the bar specimen stress law choice for the cracked plate specimen response, the quality of the choice of the stress strain curve is checked by the quality of the global force displacement law. The finite element analysis was conducted as follows: DIC was used to find the real Boundary Conditions (BCs) to be applied to the finite element model for any fracture tests for each load level. The test has then been simulated by a refined finite element plane stress analysis, using the material properties extracted from the standard stress strain curve obtained at the corresponding thermal history. The FEM predicted load displacement curve is compared to the experimental one to check the quality of the simulation as well as the adequate choice of the stress strain curve. J_{1C} value is then extracted using the elastoplastic evaluation of J . This procedure is applied for any point (A–G). Fig. 3 is a sketch of the methodology.

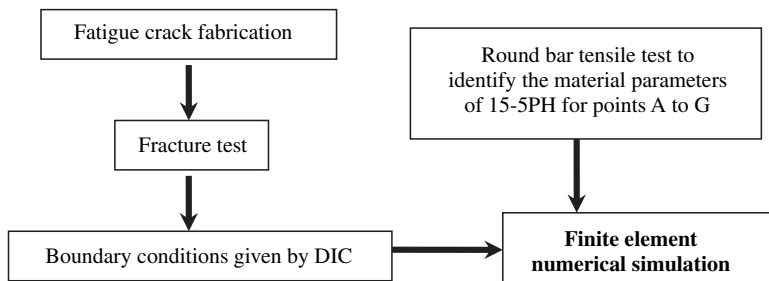


Fig. 3. Methodology to get J_{1C} from experiments.

The paper is organised as follows. One first presents the experimental setup, then the results and their analysis. The numerical simulation of experiments is then presented and compared to experimental basic results. The J_{IC} values are finally extracted from the simulations.

2. Experiments

2.1. Specimen preparation

The geometric parameters of the Single Edge Notched Plate (SENP) and round bar specimen are presented in Fig. 4. The available supplied material (cylindrical bar of 25 mm diameter) imposed a size of the specimens, which is small. The benefits of this geometry are to provide cheap specimens, which are also easy to control on temperature. Associated with induction heating, the rates of heating and cooling are higher than what you can impose in a furnace and so, much more representative of welding processes. On the other hand, the surface of gripping is small and the gradient of temperature along the axis of the specimen (far from the crack) do not allow imposing perfect boundary conditions. The two big holes of the SENP specimen are used to fix the sample, and the two small holes permit to input the current and produce a controlled fatigue crack using Potential Drop (PD) technology. The notch has been enlarged in Fig. 4 and precisely defined in Detail B. The initial fatigue crack length is measured by the PD method using Johnson's formula [27] coupled with optical microscope and DIC. Let's also note that the crack length (around 2 mm) is large compared to the size of the microstructure (approx. 0.02 mm). The ligament is small compared to the common practice for this type of tests.

2.2. Experimental devices

A servo-electro-hydraulic tension-compression machine with maximum capacity of 250 KN produces the mechanical loading. Type K thermal couples are connected to a converter for signal amplification and conversion. The force, strain and temperature signals are collected by a digital acquisition system with an acquisition rate of 10 Hz. The strains on the round bar specimen are measured by an extensometer (stick distance 15 mm). Heating is generated by electromagnetic induction, and power is supplied by a 6 KW generator. The automated configuration includes the controller, a PC, and the system software bundle. Fig. 5 shows a global view of the experiment. For DIC, two 4 Mpx cameras were placed in front of each face of the specimen to record digital images of the two sample surfaces (5 pictures/s). The Zone Of Interest (ZOI)

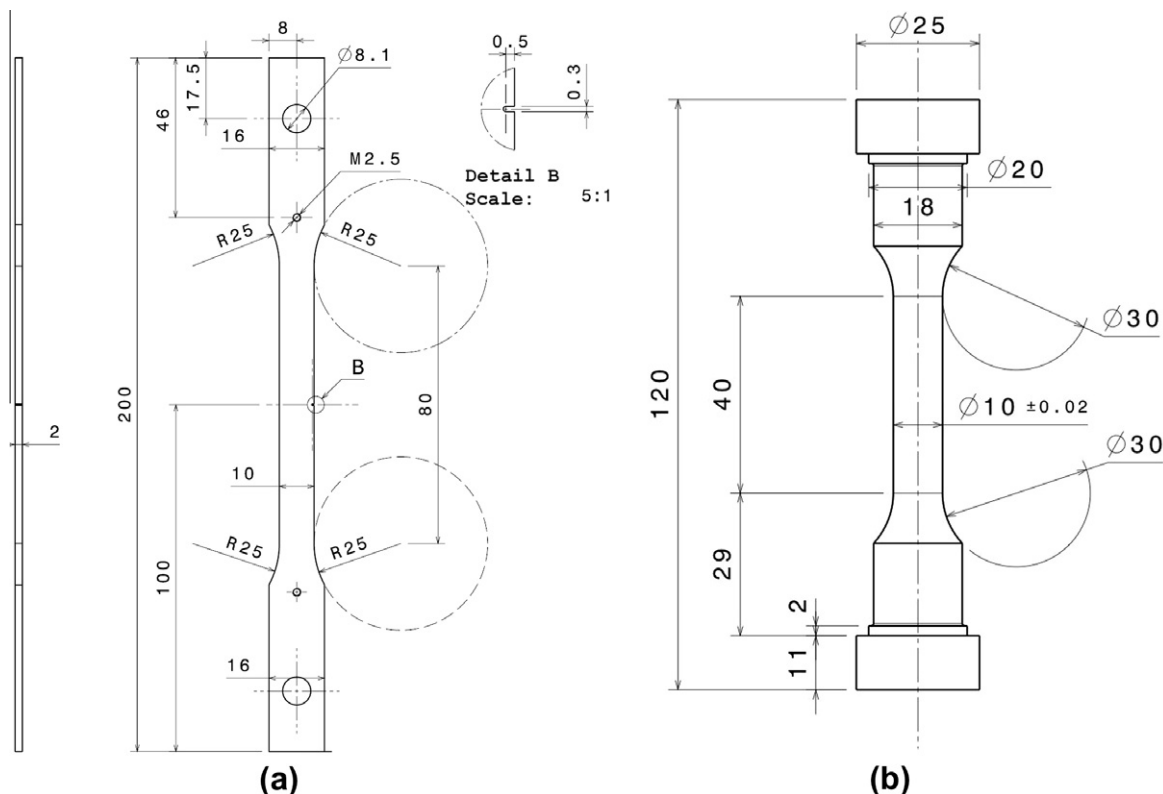


Fig. 4. Single edge notched (a) and round bar specimen (b) (all dimensions in mm).

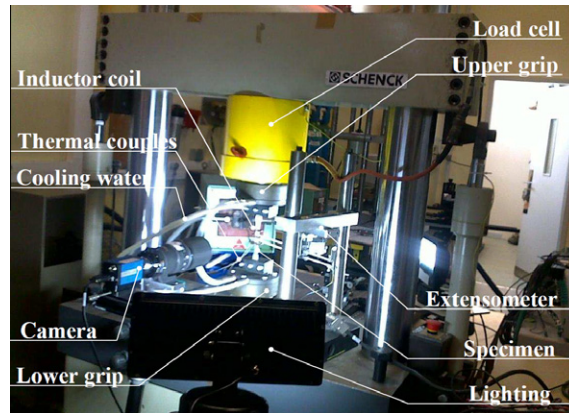


Fig. 5. Fracture test device and its installation.

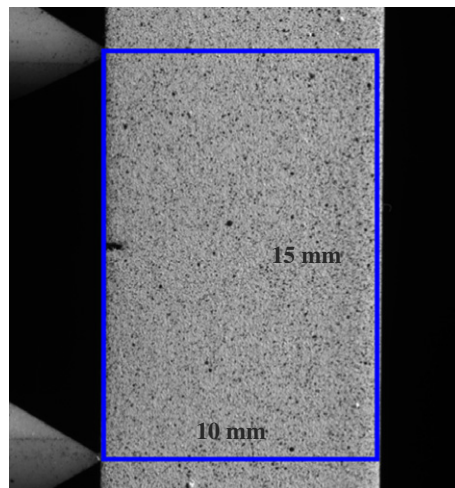


Fig. 6. ZOI on the specimen for DIC.

is chosen before the experiment and the initial pictures are taken (Fig. 6). In order to obtain good digital image of the ZOI, good illumination condition, spray paint and proper speckle pattern have been carefully chosen.

Device for round specimens is not presented here because it is very similar to the one introduced for the fracture tests.

3. Experimental results and analysis

3.1. Tensile tests results

The tensile tests were done on the round bar specimen for each points A–G. The stress–strain curves are shown in Fig. 7a where one may observe that the ultimate stress at point G is smaller than original material which is point A. Comparing curves for points B and C, the pure austenite at 200 °C (point C) is more ductile but lower strength than pure martensite (point B) at the same temperature. For points D–F, as more austenite is transformed to martensite and temperature is decreasing, the material has a higher strength. The difference between points A and B and the rest of the experiments (C–G) is that A and B have a nearly “perfect plasticity” behaviour type while the other fives show much more hardening.

3.2. Fatigue crack preparation

For each testing conditions (points A–G) at least two samples with different pre-crack length were produced. Johnson's formula, DIC, and visual microscope observation were used to get the mean value of fatigue crack length a . This procedure produces a small plastic region ahead of crack which will have to be crossed by the crack during the loading process.

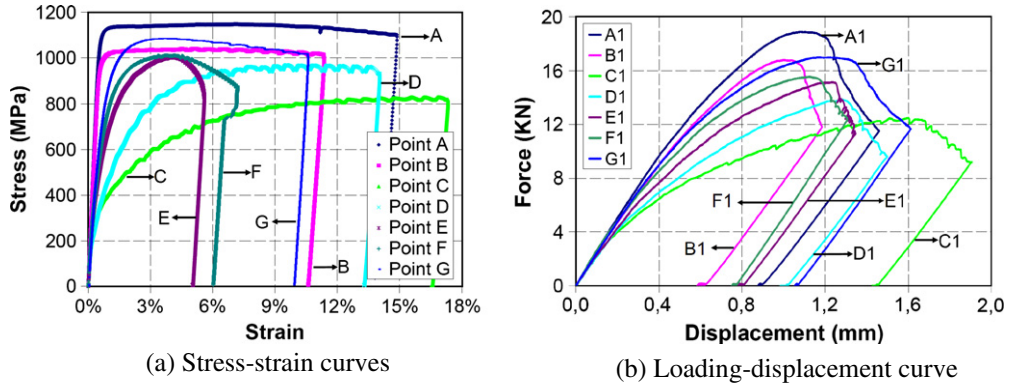


Fig. 7. Mechanical test results of 15-5PH after different heat treatment history.

Table 3
Result of fracture tests.

Experimental point	Temperature (°C)	Sample	Fatigue initial crack length (a , mm)	Maximum force of the fracture test (KN)
A	20	A1	1.654	18.87
		A2	2.060	18.51
B	200	B1	1.579	16.78
		B2	1.264	16.73
C	200	C1	1.587	11.85
		C2	2.504	10.47
D	170	D1	1.557	13.83
		D2	2.486	11.67
E	140	E1	1.566	15.12
		E2	1.249	16.33
F	110	F1	1.693	15.54
		F2	1.265	16.93
G	20	G1	1.571	16.99
		G2	1.260	17.41

3.3. Force vs. displacement curves of uniaxial fracture tests

Table 3 displays the maximum load obtained for each cracked specimen, which contains the pre-crack length of every fracture sample.

Force vs. global displacement curves of the specimens which have the similar initial crack length are plotted in Fig. 7b. The abscissa and ordinate values are given by the electro-mechanical testing machine.

One may be surprised that the maximum force of the samples with different crack length are not always consistent with the initial crack length, for example, it needs bigger force to make the sample with longer pre-crack propagate. The reason has been found to be due to a difficult control of the “grip” conditions of the specimen into the machine. This difficulty is created by the extremely simple design of the specimen with small pre-crack difference but has been solved using DIC and finite element simulation of the experiments.

3.4. Extract boundary conditions from DIC for the FEM simulation

Let us illustrate the method on specimen A1. The first point is to decide the crack propagation initial point, this was found by comparison of DIC photos and potential drop method on room temperature experiments that this point is determined by the maximum load.

Icasoft software [28] was then used to process the initial and following pictures to find the displacement field in the loading direction on top (E-PE line) and bottom (F-PF line) of the ZOI for each load step.

Fig. 8a shows the initial photo of pre-cracked specimen: the fatigue crack is difficult to see even there is no paint on the surface (a special treatment of the image in Appendix A is done to extract the crack tip from the image one must use a small load to open the crack and see its tip with DIC); (b) shows the Zone Of Interest (E-PE-F-PF): its length is 15 mm which is also the distance between the two sticks of the extensometer, its width is equal to the width of the sample which is 10 mm (c) displays the displacement field in loading direction (vertical).

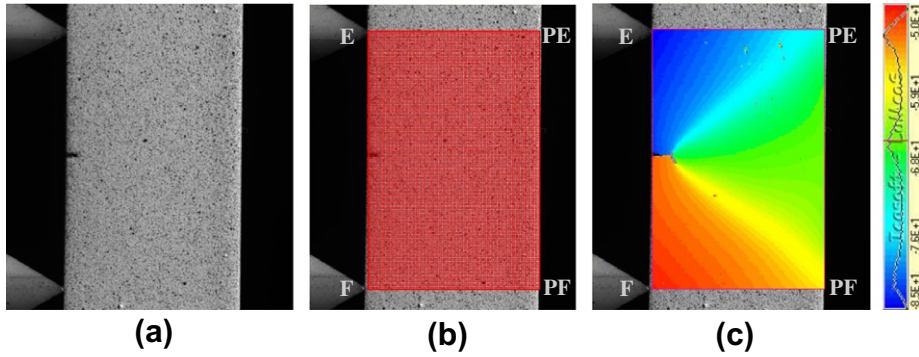


Fig. 8. Image of specimen A1, subset definition and vertical displacements fields (unit: pixel) obtained from DIC.

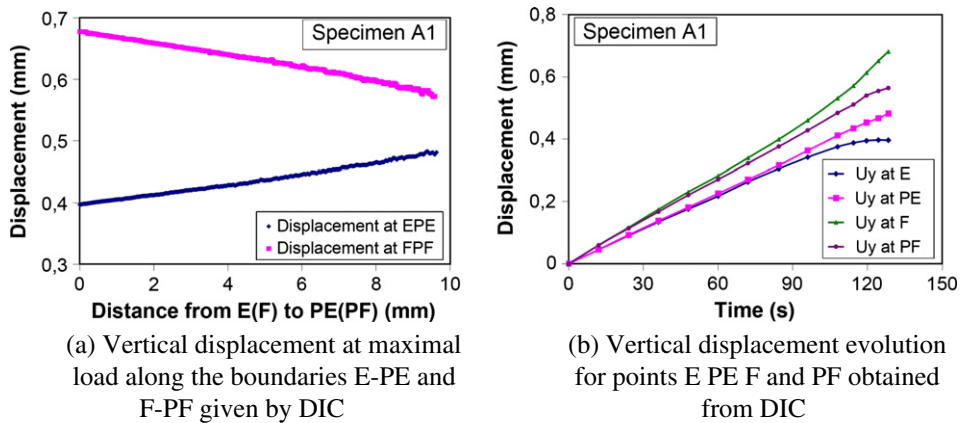


Fig. 9. Vertical displacements fields obtained from DIC for specimen A1.

DIC analysis permits to extract displacement fields along lines E-PE as well as F-PF for each picture. Fig. 9a displays the displacement obtained by DIC at the maximum force along lines E-PE and F-PF for the specimen A1. One observes that this is a straight line and that the ZOI experiences a global translation but also a rotation. This measured boundary condition can be applied at each image during the loading phase and then applied to the finite element model of the ZOI to extract directly the precise value of J_{1C} . Fig. 9b illustrates the evolution of displacements at points E, PE, F and PF up to the maximum load. The error estimated on the displacement is about 0.005 mm.

3.5. Fractography analysis

A fractography of the fracture surfaces is done by Scanning Electron Micrograph (SEM) for each specimen after failure to analyse the related fracture mechanism. It is displayed in Fig. 10.

The symbols A-G in Fig. 10 respectively are related to tests A-G. From the fractography, it is clear that each failure is characterised by a lot of microvoids. This denotes that they are all ductile fracture. 15-5PH is a high strength steel for any metallurgical state even at 200 °C or during the martensite transformation period.

When one compares the size of the microvoids, A and B have larger microvoids than others. B has bigger dimples than A. For point G, the dimples are much smaller than for case A and their density is consequently higher.

4. Numerical simulation

Large strain elastoplastic plane stress analysis was performed using CAST3M [29-31] finite element software in order to evaluate J_{1C} .

4.1. Mesh and material properties

A special attention is taken to build an appropriate mesh. It consists of a circular part of 10 layers of elements around crack tip. Quadratic 6 and 8 nodes finite elements in plane stresses are used elsewhere. Top and bottom sides are described by 10 elements as we can see in Fig. 11 where the mesh has 1358 elements.

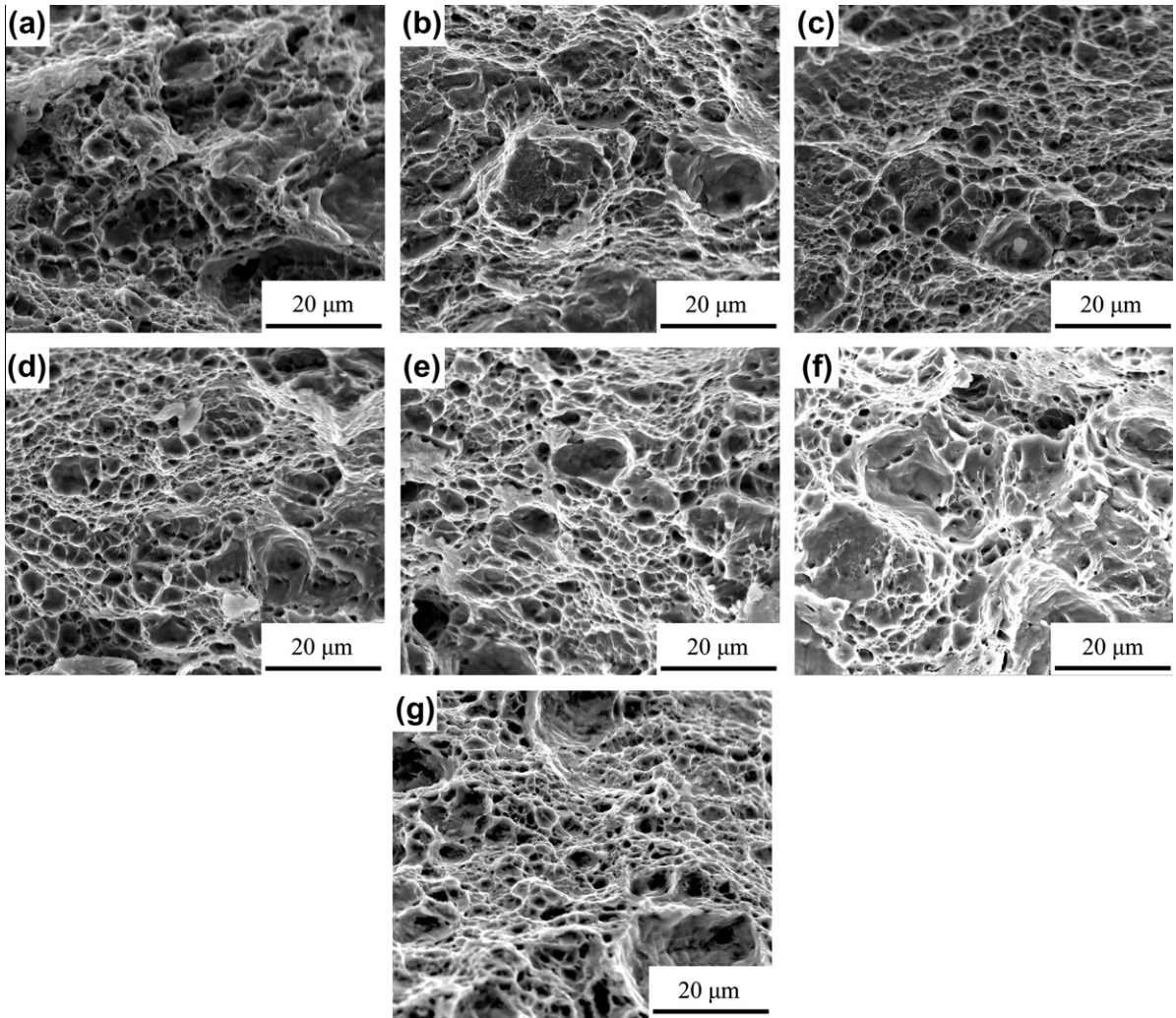


Fig. 10. Fractography of all specimens (A–G). Crack propagation direction is from the right to the left of the picture.

The size of the simulated zone is 15 mm height per 10 mm width. The material is considered to be elastoplastic with isotropic hardening. The material data are taken for each experiments from the round bar material characterisation tests done under the same heat treatment history. The measured stress–strain law is given in Fig. 7a for each case (A–G).

4.2. Boundary conditions

Translations and rotations are extracted from the experimental measured displacements histories of lines E–PE and F–PF and applied to the finite element segments EPE and FPF.

4.3. Simulation result and J_{1C} estimation

Fig. 12 shows the simulation result of displacement and accumulated plastic strain field. (a) Displays the U_y displacement which is just in the same direction to the loading and (b) presents the accumulated plastic strain around the crack tip. Fig. 13 compares the simulation result of force vs. mean displacement of two top segments of the ZOI with the experimental result for case A. The agreement is excellent which confirms the quality of the numerical simulation. Appendix A contains the same comparison for each case (B–G). One can observe that the comparison is very good in each case.

After the simulation, J_{1C} is extracted using the G_θ method [32,33], which permits to compute the energy release rate for elastoplastic radial loading. For each case (A–G) one has a number of tests available which have all been computed, thus allowing an estimation of the error on the corresponding J_{1C} . The synthesis of the analysis is given in Table 4. Fig. 14 displays the mean J_{1C} estimated value for each experimental case (A–G).

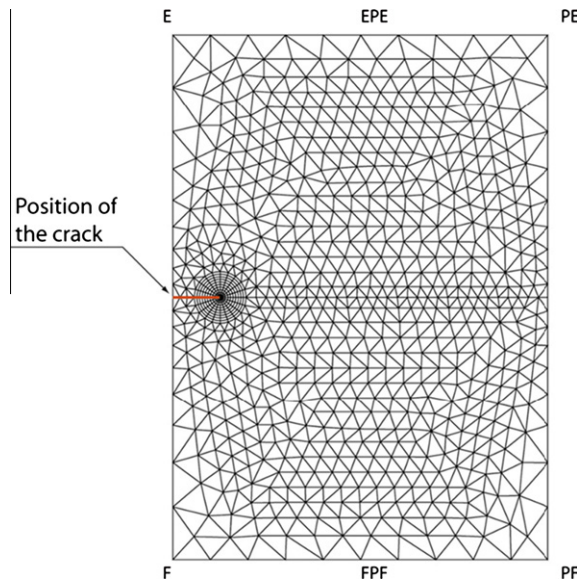


Fig. 11. Mesh used with CAST3M.

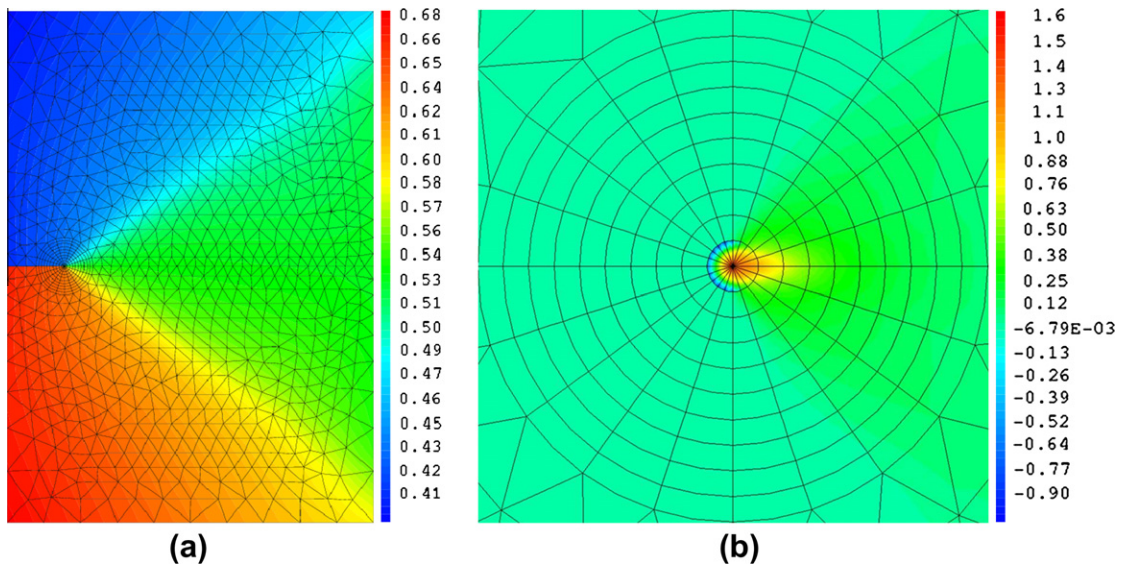


Fig. 12. Simulation result, (a) is U_y displacement field (unit: mm) and (b) is the equivalent cumulated plastic strain around crack tip.

5. Discussion

The result presented in Fig. 14 shows that the heat treatment and metallurgic phase transformation has an influence on the fracture toughness of 15Cr–5Ni stainless steel.

If one compares cases A and B, which are fully martensitic, but at different temperature, A has a bigger J_{1C} value than B. The reason is not obvious. The difference is of about 20%. This observation should be confirmed by a larger number of experiments.

One now compares the toughness at 200 °C but with two distinct metallurgic states: cases B (fully martensitic) and C (fully austenitic provided the martensitic transformation is over when the tensile test is performed). J_{1C} for case B is clearly smaller than the one of case C. 15–5PH in austenitic phase is tougher than in martensitic one.

Comparing the toughness J_{1C} of cases A and G, the material after a whole cycle heat treatment has a higher fracture toughness than the original material. This should be due to some residual austenite in the material after the heat treatment. This is confirmed by the fractographic analysis of the failure zone which shows a more ductile fracture mode.

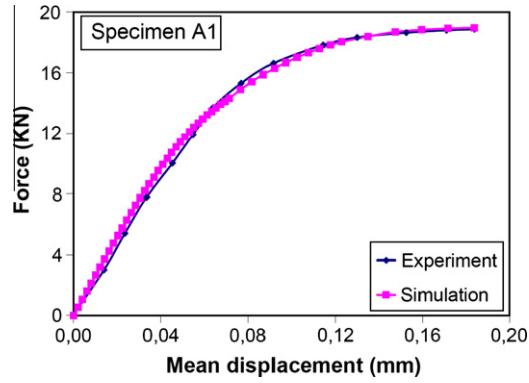


Fig. 13. The force vs. mean displacement of specimen A1 at point A.

Table 4

Critical J -integral results of all samples.

Experimental point	Temperature (°C)	Sample	J_{1C} (kJ/m ²)	Mean J_{1C} (kJ/m ²)
A	20	A1	247	259
		A2	270	
B	200	B1	190	186
		B2	182	
C	200	C1	298	318
		C2	337	
D	170	D1	239	258
		D2	276	
E	140	E1	292	252
		E2	211	
F	110	F1	269	263
		F2	257	
G	20	G1	306	315
		G2	323	

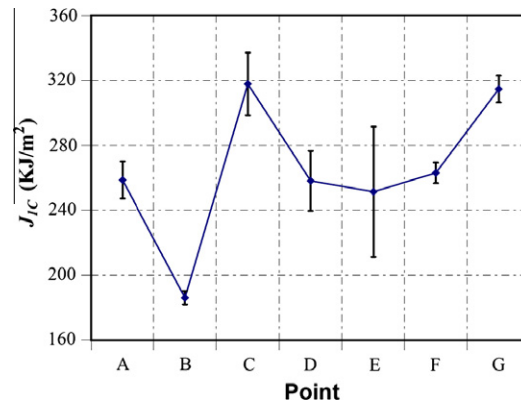


Fig. 14. J_{1C} of 15-5PH at different temperature.

For cases D–F, both martensite and austenite phase (their proportion is given in Table 2) co exist in the specimens. Globally the toughness is smaller during the phase transformation than when it is finished or not started. But the decrease is not huge.

Overall, one can conclude that austenite enhance the ductility and then the toughness J_{1C} of the material. Let us also observe that these experiments do not give enough information for the evaluation of the pertinence of a mixture rule between austenite and martensite toughnesses.

6. Conclusions

This paper proposed a simple and effective method which mixes Digital Image Correlation (DIC) and finite element numerical simulation to extract the J_{IC} value of 15–5PH at different metallurgical states enhanced by typical welding or repair temperature cycles. The fractography is also analysed to understand the reasons of the evolution of energy release rate or crack growth resistance. The effect of thermal history was studied through the analysis of the evolution of toughness of seven points. The effect of the austenite phase transformation on the mechanical behaviour of 15–5PH was studied. The J_{IC} value shows that the pure martensite 15–5PH at room temperature has smaller fracture toughness than after a whole heat treatment: the fracture toughness increase is probably caused by some residual austenite. Moreover pure austenite 15–5PH at 200 °C has a higher fracture toughness than pure martensite 15–5PH at the same temperature. For the dual phase 15–5PH observed during the austenite–martensite phase transformation, the observed relative loss of toughness is around 20%, it is real but not as huge as expected. The value of toughness are evaluated using non standard procedures with a low triaxiality which may lead to some overestimation.

Acknowledgements

The authors are grateful to Dr. T Wu for his initial development work and express our gratitude to Mr. Georges. Hugueny from INSA.CEREP for machining the sample.

References

- [1] Wu T. Experiment and numerical simulation of welding induced damage of stainless steel 15–5PH. Ph.D. thesis. France: INSA de Lyon; 2007.
- [2] Hsu TY. Martensite transformation and martensite. 2nd ed. Beijing: Science Press; 1999. p. 556–64.
- [3] Hamata N. Modelisation du Couplage Entre L'elasto-viscoplasticite Ansotherme et la Transformation de Phase D'un Fontr G.S. Ferritique. These de Doctorat de L'universite Paris 6; 1992.
- [4] Hashin Z, Shtrikman S. A variational approach to the theory of the effective magnetic permeability of multiphase materials. *J Appl Phys* 1962;33:3125–31.
- [5] Coret M, Calloch S, Combescure A. Experimental study of the phase transformation plasticity of 16MND5 low carbon steel under multiracial loading. *Int J Plast* 2002;18:1707–27.
- [6] Greenwood GW, Johnson RH. The deformation of metals under small stresses during phase transformation. *Proc Royal Soc* 1965;283:403–22.
- [7] Magee CL. Transformation kinetics, microplasticity and ageing of martensite in Fe-31–Ni. Ph.D. thesis. Pittsburgh: Carnegie Mellon University; 1966.
- [8] Bressanelli JP, Moskowitz A. Effects of strain rate, temperature and composition on tensile properties of metastable austenitic stainless steels. *ASM Trans Quart* 1966;5(9):223.
- [9] Zackay VF, Parker ER, Fahr D, Busch R. The enhancement of ductility in high-strength steels. *Trans ASM* 1967;60:252.
- [10] Gerberich WW, Hemmings PB, Merz MD, Zackay VF. Preliminary toughness results on TRIP steel. *ASM Trans Quart* 1968;61:843.
- [11] Gerberich WW, Hemmings PB, Zackay VF, Parker ER. Interactions between crack-growth and strain-induced transformation, fracture. London: Chapman and Hall Ltd.; 1969. p. 288.
- [12] Antolovich SD, Singh B. On the toughness increment associated with the austenite to martensite phase transformation in TRIP steels. *Met Trans* 1971;2:2135.
- [13] Pati SR, Cohen M. Nucleation of the isothermal martensitic transformation. *Acta Metall* 1969;1(7):189.
- [14] Raghavan V, Cohen M. Measurement and interpretation of isothermal martensitic kinetics. *Met Trans* 1971;2:2409.
- [15] Sun Q-P, Hwang K-C. Micromechanics modelling for the constitutive behavior of polycrystalline shape memory alloys. *J Mech Phys Solids* 1993;41:1–33.
- [16] Hannink RHJ, Kelly PM, Muddle BC. Transformation toughening in zirconia-containing ceramics. *J Am Ceram Soc* 2000;83:461–87.
- [17] Yan Wenyi, Wang Chun Hui, Zhang Xin Ping, Mai Yiu-Wing. Effect of transformation volume contraction on the toughness of super elastic shape memory alloys. *Smart Mater Struct* 2002;11:947–55.
- [18] Rice JR. Fracture. Academic Press; 1968. p. 191–311.
- [19] Begley JA, Landes JD. The J integral as a fracture criterion in fracture toughness: 1971. Proceedings, Part II. ASTM STP 1972;514:1–20.
- [20] Yoda M. The J -integral fracture toughness for Mode II. *Int J Fract* 1980;16(4):R175–8.
- [21] Wilson Christopher D, Mani Prabhu. Plastic J -integral calculations using the load separation method for the double edge notch tension specimen. *Engng Fract Mech* 2008;75:5177–86.
- [22] Dietmar Gross, Thomas Seeling. Fracture mechanics with an introduction to micromechanics. Springer; 2006. p. 156–9.
- [23] Kumar V, German MD, Shih CF. An engineering approach for elastic–plastic fracture analysis. EPRI Report NP 1931; 1981.
- [24] ASTM E1820. Standard test method for measurement of fracture toughness, annual book of ASTM standards. Philadelphia (PA): ASTM; 2001.
- [25] Mguil-Touchal S, Morestin F, Brunet M. Various experimental applications of digital image correlation method. *CMEM Rhodes* 1997; 45–58.
- [26] Thorsten Siebert, Crompton Matt J, Brunet M. Application of high speed digital image correlation for vibration mode shape analysis. In: Proceedings of the SEM annual conference, Indianapolis, Indiana, USA, June 7–10, 2010.
- [27] Johnson HH. Calibrating the electric potential method for studying slow crack growth. *Mater Res Stand* 1965:442–5.
- [28] LaMCoS. UMR CNRS 5259. INSA de Lyon (ICASOFT, digital image correlation software). <<http://icasoft.insa-lyon.fr/>>
- [29] Andrei Constantinescu. An introduction to finite elements based on examples with Cast3m. Laboratoire de Mécanique des Solides CNRS UMR 7649, Département de Mécanique, Ecole Polytechnique, 91120 Palaiseau, France. <<http://catalogue.polytechnique.fr/site.php?id=556&fileid=4547>>.
- [30] Le Fichoux E. Présentation et Utilisation de CASTEM 2000, ENSTA 1998.
- [31] Fleuret JS. Prise en main de CASTEM 2000 par l'exemple, CEA Saclay/DRN/DMT/SEMT/LAMS 1996.
- [32] Destuynder P, MDjoua, Lescure S. Some remarks on elastic fracture mechanics. *J Mech Théor Appl* 1983;2:113–35.
- [33] Suo XZ, Combescure A. Second variation of energy and an associated line independent integral in fracture mechanics. *Eur J Mech A: Solids* 1992;11:609–24.